Mechanistic Study of Cast and 3D-Printed Stainless Steel Electropolishing in Acid Media and Deep Eutectic Solvents

Chloé Rotty, Marie-Laure Doche, Audrey Mandroyan, Vincent Vivier, Jean-Yves Hihn

Mechanistic study of cast and 3D-printed stainless steel electropolishing in acid media and deep eutectic solvents

Chloé Rotty[a], Marie-Laure Doche[a], Audrey Mandroyan[a], Vincent Vivier[b,*], Jean-Yves Hihn[a,**]

[a] *Institut UTINAM, UMR CNRS 6213, Université de Bourgogne Franche-Comté, 30 avenue de l'Observatoire, 25 009 Besançon, France*
[b] *Sorbonne Université, CNRS, Laboratoire de Réactivité de Surface, 4 place Jussieu, 75005, Paris, France*

Abstract

The mechanistic analysis of the electropolishing procedure of stainless steel (SS) was revisited using electrochemical impedance spectroscopy. Firstly, the control of the dissolution reaction by diffusion was confirmed with the linear dependence of the limiting current density as a function of the electrode rotation rate using the Levich's law. Nevertheless, varying the viscosity (by changing temperature from 35°C to 70°C) show a direct relationship between the diffusion coefficient and the kinematic viscosity, irrespective of the cation concentration at the interface, thus suggesting a minor role in the diffusion limiting step. This limitation is therefore provided by the diffusion of an acceptor specie from the electrolyte toward the anode surface. To discriminate the role of water or mineral anion in the so-called acceptor model, a full descriptive model of the electrochemical behaviour of interface was devised for analyzing electropolishing results obtained by electrochemical impedance spectroscopy (EIS) for both cast and additive layer manufactoring (ALM) 316L SS in aqueous acid electrolyte and in deep eutectic solvent (DES). It was shown that the model involving an acceptor specie allows to describe with a good accuracy the electrochemical behavior of the different systems at several potentials.

Keywords: Electrochemical impedance spectroscopy, Ionic liquid, Electrochemical dissolution, Surface treatment, Additive manufacturing

*vincent.vivier@sorbonne-universite.fr (Vincent Vivier)
**jean-yves.hihn@univ-fcomte.fr (Jean-Yves Hihn)

1. Introduction

Over the last decades, innovative manufacturing processes [1, 2, 3] has emerged, enabling the production of metal workpieces with both complex shapes and sophisticated internal structures such as fluid flow channels [4]. Among all the available techniques, Additive Layer Manufacturing (ALM) and more specifically Selective Laser Melting (SLM) consists in fabricating 3-dimensional objects by successively adding material layer by layer [5, 6]. These manufacturing processes are a complete break with conventional ones based on a subtractive approach such as machining. Typical SLM processes can be considered as fast solidification processes during which temperature gradients generate complex macro and microstructures [7]. Moreover, the surface appearance of the metal workpieces may be indeed of poor quality (depending on metallic powder characteristics) compared to that obtained when the workpieces come out of machining. The direct use of additive manufacturing parts without a finishing stage is therefore often not possible, which requires the implementation of a subsequent surface treatment step.

Electropolishing (EP) process is now extensively considered as post-traitement particularly for additive manufacturing parts. This wet electrolytic process consists in a controlled dissolution of metallic surfaces leading to a decrease of the surface roughness which is usually accompanied by a brightness increase [8, 9]. Unlike the other mechanical polishing techniques, EP process does not induce any residual stresses since the metal layers on the surface are not hardened, but softly removed by electrochemical dissolution. The main problem in carrying out this oxidation reaction is to determine the most suitable electrolyte composition and experimental conditions. Although this process is usually carried out in concentrated acidic media, alternative environmentally-friendly electrolytes have been developed in recent years such as Deep Eutectic Solvents (DESs) [10, 11, 12] or in sulfuric acid free electrolyte [13], depending on the type of metal.

It has already been reported in several papers that three to four distinct regions can be seen on a typical electropolishing polarization curve [14, 15, 16]. Starting from the corrosion potential and moving towards more anodic potentials, the first domain is ascribed to active dissolution of the

substrate after oxide layer breakdown. The second region refers to a viscous film formation at the electrolyte/substrate interface, but is not always seen on the current/potential curve. The third region is the limiting current plateau and is characteristic of a diffusion controlled mechanism: this is the electropolishing zone. The fourth region for the higher overpotential, corresponds to solvent oxidation and oxygen evolution reactions.

Studies have shown that levelling can be carried out under primary current distribution (i.e., controlled by ohmic drop), secondary current distribution (controlled by charge transfer considering that concentration gradient are negligible) and tertiary current distribution (controlled by mass transfer) [17, 18, 19]. Brightening is only possible when dissolution is limited by mass transfer and when a homogeneous layer covers the surface. It should be noticed that these EP description and analysis were mainly developed to account for the profile shape of the material surface and the geometry of the electrochemical cell, independently of the dissolution mechanism itself.

Following the seminal works of Jacquet [20, 21], Elmore [22, 23] and Wagner [24], Edwards [25, 26] developed a model accounting for an acceptor species such as anion or solvent molecules that complex the metal cation, thus controlling the rate of the dissolution. Matlosz [27] developed the mathematical expression of the electrochemical impedance accounting for the physical bases for salt film and acceptor models. This general description provided a first approach for the mechanistic analysis based on the analysis of the shape of the Nyquist diagrams, but the electrochemical reaction was described as simple charge transfer reaction, neglecting possible formation of adsorbate nor taking into account more complex chemical steps.

Based on steady-state and EIS measurements, Bojinov et al. introduced a kinetic model for describing the passivation mechanism of iron in concentrated phosphoric solution [28]. Interestingly, this mechanism involves surface intermediates leading to the formation of Fe(II) and Fe(III), whereas the formation of Fe(I) was assumed to be negligible. Conversely, using electrohydrodynamic impedance for a fine investigation of the mass transfer contribution mechanism in sulphuric acid solution, Barcia et al. developed a model accounting for the formation of a thin film with a viscosity profile spreading from the electrode surface to the bulk solution, which also involves

monovalent and divalent Fe intermediates [29]. Additionally, one can expect different time constants in the EIS response depending on the metal and the electrolyte.

Given the complexity of the electropolishing process, many mechanisms have also been proposed for steel. In this respect, this work focuses on the electropolishing mechanism, which has been investigated by Linear Sweep Voltammetry (LSV) and Electrochemical Impedance Spectroscopy (EIS) for cast and ALM 316L Stainless Steel in both concentrated phosphoric and sulphuric acid media and choline chloride-ethylene glycol mixtures. To discriminate the role of water or mineral anion, a full descriptive model of the electrochemical behaviour of interface was developed. This model found its roots in iron dissolution and electropolishing considerations. EIS measurements were carried out in acidic and DES media in order to confront experimental results with the simulations of the dissolution reaction. In the first case, water was assumed to be the limiting specie and in the second case an acceptor specie (such as phosphates or chlorides) was considered. The same study has been performed for both cast and additive manufacturing 316L Stainless Steel. In all cases, the proposed model allows to describe with a good accuracy the electrochemical behaviour of the EP process at different potentials.

2. Experimental

The working electrodes consisted of a 316L stainless steel disk electrodes of 3.5 mm in diameter (9.62 mm^2) of both cast or additive layer manufacturing metals, the compositions of which are given in Table 1. Before each experiment, the electrode surface was mechanically polished with abrasive SiC paper (P1200), rinsed with alcohol and dried with compressed air. Then, the material was mounted on a rotating-disk electrode (RDE).

Table 1: Elemental composition of the alloys

Composition (wt.%)	Fe	Cr	Ni	Mo	Mn
Cast 316L	67.7	17.3	11.4	2.1	1.5
ALM 316L	66.8	17.4	11.7	3.9	0.1

The electrolyte solutions consisted of either a mixture of 45% H_3PO_4, 35% H_2SO_4 and 20% H_2O or a choline chloride (ChCl) + ethylene glycol (EG) in a molar ratio (1:2). The physicochemical properties of both solvents used in this work are presented in Table 2. Electrochemical experiments were carried out in a jacketed glass reactor for controlling the temperature within a 3-electrode configuration. The electrolyte temperature was regulated at 70 ± 1°C and the volume of electrolyte for each experiment was 200 mL. The electrochemical experiments (polarization curves, electrochemical impedance spectroscopy diagrams) were performed with a SP 240 potentiostat (Bio-Logic). The counter and reference electrodes were a large area platinized titanium grid facing the working electrode and a saturated calomel reference electrode (E_{SCE} = 0.241 V/SHE), respectively. EP procedure was carried out under a potentiostatic control at different potentials. Each EIS measurement was performed after the polarization of the sample for 1 minute. The frequency domain investigated was 1 MHz down to 100 mHz, with 10 points per decade of frequency and a sine wave amplitude of 10 mV_{rms}.

Table 2: Physicochemical properties of the solvents used for the electropolishing procedure

	T / °C	ρ / g cm^{-3}	η / mPa s	σ / mS cm^{-1}
45% H_3PO_4 + 35% H_2SO_4 + 20% H_2O	25	1.56	6.88	178.3
	70	1.548	2.79	324.9
ChCl + EG (1:2)	25	1.116	31.35	9.04
	70	1.097	7.88	30.05

3. Models for the electropolishing

3.1. Model

In this work, electrochemical polishing is described by successive elemental one-electron reactions as previously done for the study of the dissolution mechanism of different metals [30, 31, 32, 33], M, and accounting for the formation of adsorbed species as reaction intermediates.

$$M \xrightarrow{K_1} M^+_{ads} + e^- \quad (1)$$

$$\mathrm{M}^{+}_{\mathrm{ads}} + \mathrm{A} \xrightarrow{K_2} \mathrm{MA}^{2+}_{\mathrm{ads}} + \mathrm{e}^{-} \tag{2}$$

in which A is a species used to complex metal cations, and K_1 and K_2 are the reaction rates of the electrochemical reactions which are exponentially potential dependent (Tafel's law) and express as

$$K_1 = k_1 e^{\left(\frac{\alpha_1 F}{RT} E\right)} \tag{3}$$

$$K_2 = k_2 e^{\left(\frac{\alpha_2 F}{RT} E\right)} \tag{4}$$

where E is the electrode potential (in V), k_1 and k_2 are the potential independent reaction rates of each step, α_1 and α_2 are the charge transfer coefficients, and F, R, and T are the Faraday constant (96485 C mol^{-1}), the gas constant (8.314 J K^{-1} mol^{-1}), and the temperature (in K), respectively. It is also interesting to note that this mechanism involves the dissolution of metals in the form of divalent ions, i.e. we assume that the chromium in the steel contributes little or nothing to the impedance response. Additionally, we assume that the adsorption isotherms corresponding to the formation / consumption of reaction intermediates M^{+}_{ads} and MA^{2+}_{ads} obey a Langmuir isotherm and are characterized by the surface coverages θ_1 and θ_2, respectively. The last step is the dissolution of the adsorbed complex formed at the electrode surface, MA^{2+}_{ads}, which can be expressed as

$$\mathrm{MA}^{2+}_{\mathrm{ads}} + \mathrm{B} \xrightarrow{k_d} \mathrm{MAB}^{2+} \tag{5}$$

where k_d is the kinetic constant of the chemical reaction, and B a species, such as a water molecule, which promotes the dissolution of the metal complex MA^{2+}_{ads}. At this point, it is interesting to mention that the species A is considered to be the acceptor species for complexing the metal cations (*i.e.* phosphate type species) and species B is considered to be the water molecules contained in the solvent, but in both cases, the concentrations of A and B at the electrode surface are controlled by diffusion. As previously described in the literature, two hypotheses can be formulated a priori concerning the nature of the limiting step in the EP process: either A or B is the limiting species, but in both cases the concentration of the other species remains constant at the electrode surface.

3.2. Derivation of the impedance expression

The rates of the 3 reactions (1),(2), and (5) are given by

$$v_1 = K_1 \left(1 - \theta_1 - \theta_2\right) \tag{6}$$

$$v_2 = K_2 \left[A\right]_0 \theta_1 \tag{7}$$

$$v_3 = k_d \left[B\right]_0 \theta_2 \tag{8}$$

The time evolution relationship for surface coverages express as

$$\beta \frac{d\theta_1}{dt} = v_1 - v_2 = K_1 \left(1 - \theta_1 - \theta_2\right) - K_2 \left[A\right]_0 \theta_1 \tag{9}$$

$$\beta \frac{d\theta_2}{dt} = v_2 - v_3 = K_2 \left[A\right]_0 \theta_1 - k_d \left[B\right]_0 \theta_2 \tag{10}$$

where β is the surface concentration for complete coverage (in mol cm^{-2}). At steady-state, the surface coverage for each species is constant, and thus

$$\frac{d\theta_1}{dt} = 0 \tag{11}$$

and

$$\frac{d\theta_2}{dt} = 0 \tag{12}$$

leading to the set of equations

$$\begin{cases} K_1 \left(1 - \theta_1 - \theta_2\right) - K_2 \left[A\right]_0 \theta_1 = 0 \\ K_2 \left[A\right]_0 \theta_1 - k_d \left[B\right]_0 \theta_2 = 0 \end{cases} \tag{13}$$

allowing the steady-state surface coverages, $\overline{\theta}_1$ and $\overline{\theta}_2$, to be expressed as

$$\overline{\theta}_1 = \frac{K_1 k_d \left[B\right]_0}{K_1 k_d \left[B\right]_0 + K_1 K_2 \left[A\right]_0 + K_2 \left[A\right]_0 k_d \left[B\right]_0} \tag{14}$$

$$\overline{\theta}_2 = \frac{K_1 K_2 \left[A\right]_0}{K_1 k_d \left[B\right]_0 + K_1 K_2 \left[A\right]_0 + K_2 \left[A\right]_0 k_d \left[B\right]_0} \tag{15}$$

where $\left[A\right]_0$ and $\left[B\right]_0$ are the concentration of A and B at the electrode surface, respectively.

The faradaic current is given by the algebraic sum of each electrochemical contribution (on the anodic domain, the cathodic contribution to the current was neglected)

$$i = F \left(v_1 + v_2\right) \tag{16}$$

$$i = F\left[K_1\left(1-\theta_1-\theta_2\right)+K_2\left[A\right]_0\theta_1\right] \tag{17}$$

thus allowing the equation of the steady-state polarization curve to be derived

$$i = F\left[K_1\left(1-\overline{\theta}_1-\overline{\theta}_2\right)+K_2\left[A\right]_0\overline{\theta}_1\right] \tag{18}$$

The faradaic impedance, Z_f, is obtained from the first order of the Taylor expansion of the current, which can be expressed in the Laplace domain as

$$\begin{aligned}\frac{1}{Z_f(p)} = \frac{\Delta i(p)}{\Delta E(p)} &= \left(\frac{\partial i}{\partial E}\right)_{\theta_1,\theta_2,[A]_0} + \left(\frac{\partial i}{\partial \theta_1}\right)_{E,\theta_2,[A]_0}\frac{\Delta\theta_1(p)}{\Delta E(p)} \\ &+ \left(\frac{\partial i}{\partial \theta_2}\right)_{E,\theta_1,[A]_0}\frac{\Delta\theta_2(p)}{\Delta E(p)} + \left(\frac{\partial i}{\partial \left[A\right]_0}\right)_{E,\theta_1,\theta_2}\frac{\Delta\left[A\right]_0(p)}{\Delta E(p)}\end{aligned} \tag{19}$$

where p is the variable in the Laplace domain $p \equiv j\omega$, where $j = \sqrt{-1}$, ω is the angular frequency ($\omega = 2\pi f$), and f the frequency in Hz. Each partial derivative can then be evaluated a function of the model parameters as

$$\left(\frac{\partial i}{\partial E}\right)_{\theta_1,\theta_2,[A]_0} = F\left[\frac{\alpha_1 F}{RT}K_1\left(1-\theta_1-\theta_2\right)+\frac{\alpha_2 F}{RT}K_2\left[A\right]_0\theta_1\right] \tag{20}$$

$$\left(\frac{\partial i}{\partial \theta_1}\right)_{E,\theta_2,[A]_0} = F\left(K_2\left[A\right]_0 - K_1\right) \tag{21}$$

$$\left(\frac{\partial i}{\partial \theta_2}\right)_{E,\theta_1,[A]_0} = -FK_1 \tag{22}$$

$$\left(\frac{\partial i}{\partial \left[A\right]_0}\right)_{E,\theta_1,\theta_2} = FK_2\theta_1 \tag{23}$$

Additionally, from the linearization of Eqs.(9) and (10) it comes

$$\begin{aligned}j\omega\beta\Delta\theta_1 = &\left[\frac{\alpha_1 F}{RT}K_1\left(1-\theta_1-\theta_2\right)-\frac{\alpha_2 F}{RT}K_2\left[A\right]_0\theta_1\right]\Delta E \\ &-\left(K_1+K_2\left[A\right]_0\right)\Delta\theta_1 - K_1\Delta\theta_2 - K_2\theta_1\Delta\left[A\right]_0\end{aligned} \tag{24}$$

$$\begin{aligned}j\omega\beta\Delta\theta_2 = &\frac{\alpha_2 F}{RT}K_2\left[A\right]_0\theta_1\Delta E + K_2\left[A\right]_0\Delta\theta_1 - k_d\left[B\right]_0\Delta\theta_2 \\ &-k_d\theta_2\Delta\left[B\right]_0 + K_2\theta_1\Delta\left[A\right]_0\end{aligned} \tag{25}$$

For sake of simplicity, the thickness of the diffusion layer, δ, for both diffusing species, is expressed as

$$\delta = 1.61 D_s^{1/3}\Omega^{-1/2}\nu^{1/6} \tag{26}$$

where D_s is the diffusion coefficient of the species s (in cm^2 s^{-1}), Ω the rotation rate of the RDE (in rad s^{-1}), and ν the kinematic viscosity (in cm^2 s^{-1}). The concentration of diffusing species can be obtained from the solution of the second Fick's law under the assumption of diffusion through a film with exchange of electroactive species between the film and the electrolyte (transmissive boundary condition) [34, 35].

$$\frac{\Delta [A]_0}{\Delta i} = \frac{1}{FD_A} \frac{tanh\left(\delta\sqrt{\frac{j\omega}{D_A}}\right)}{\sqrt{\frac{j\omega}{D_A}}} \tag{27}$$

$$\frac{\Delta [B]_0}{\Delta i} = \frac{1}{FD_B} \frac{tanh\left(\delta\sqrt{\frac{j\omega}{D_B}}\right)}{\sqrt{\frac{j\omega}{D_B}}} \tag{28}$$

It is worth mentioning that A and B do not play a symmetrical role in the EP mechanism as shown by Eqs. (1), (2), and (5), and thus at this point, two cases have to be envisioned for the derivation of the analytical expression of the impedance: either B is the limiting species and it is assumed that the concentration of A remains constant in the whole electrolyte, including at the electrode surface, either A is the limiting species and it is assumed that the concentration of B remains constant in the electrolyte.

3.2.1. B is the limiting species

Assuming that B is the limiting species, Eq.(28) expresses as

$$\frac{\Delta [B]_0}{\Delta E} = \frac{1}{Z_f} \frac{1}{FD_B} \frac{tanh\left(\delta\sqrt{\frac{j\omega}{D_B}}\right)}{\sqrt{\frac{j\omega}{D_B}}} \tag{29}$$

and Eqs.(19), (24) and (25) can be written as linear system of equations

$$\begin{cases} (j\omega\beta + K_1 + K_2 [A]_0) \frac{\Delta\theta_1}{\Delta E} + K_1 \frac{\Delta\theta_2}{\Delta E} = \\ \qquad \left[\frac{\alpha_1 F}{RT} K_1 (1 - \theta_1 - \theta_2) - \frac{\alpha_2 F}{RT} K_2 [A]_0 \theta_1\right] \\ -K_2 [A]_0 \frac{\Delta\theta_1}{\Delta E} + (j\omega\beta + k_d [B]_0) \frac{\Delta\theta_2}{\Delta E} + \frac{k_d \theta_2}{FD_B} \frac{tanh\left(\delta\sqrt{\frac{j\omega}{D_B}}\right)}{\sqrt{\frac{j\omega}{D_B}}} \frac{1}{Z_f F} = \\ \qquad \frac{\alpha_2 F}{RT} K_2 [A]_0 \theta_1 \\ F (K_1 - K_2 [A]_0) \frac{\Delta\theta_1}{\Delta E} + FK_1 \frac{\Delta\theta_2}{\Delta E} + \frac{1}{Z_f F} = \\ \qquad F\left[\frac{\alpha_1 F}{RT} K_1 (1 - \theta_1 - \theta_2) + \frac{\alpha_2 F}{RT} K_2 [A]_0 \theta_1\right] \end{cases} \tag{30}$$

The faradaic impedance is then obtain as a solution of this system of 3 linear equations.

3.2.2. A is the limiting species

Assuming that A is the limiting species, Eq.(27) expresses as

$$\frac{\Delta [A]_0}{\Delta E} = \frac{1}{Z_f} \frac{1}{F D_A} \frac{tanh\left(\delta \sqrt{\frac{j\omega}{D_A}}\right)}{\sqrt{\frac{j\omega}{D_A}}} \tag{31}$$

and Eqs.(19), (24) and (25) can be written as linear system of equations

$$\begin{cases} \left(j\omega\beta + K_1 + K_2 [A]_0\right) \frac{\Delta\theta_1}{\Delta E} + K_1 \frac{\Delta\theta_2}{\Delta E} + \frac{K_2\theta_1}{F D_A} \frac{tanh\left(\delta\sqrt{\frac{j\omega}{D_A}}\right)}{\sqrt{\frac{j\omega}{D_A}}} \frac{1}{Z_f F} = \\ \qquad \left[\frac{\alpha_1 F}{RT} K_1 (1 - \theta_1 - \theta_2) - \frac{\alpha_2 F}{RT} K_2 [A]_0 \theta_1\right] \\ -K_2 [A]_0 \frac{\Delta\theta_1}{\Delta E} + \left(j\omega\beta + k_d [B]_0\right) \frac{\Delta\theta_2}{\Delta E} - \frac{K_2\theta_1}{F D_A} \frac{tanh\left(\delta\sqrt{\frac{j\omega}{D_A}}\right)}{\sqrt{\frac{j\omega}{D_A}}} \frac{1}{Z_f F} = \\ \qquad \frac{\alpha_2 F}{RT} K_2 [A]_0 \theta_1 \\ F\left(K_1 - K_2 [A]_0\right) \frac{\Delta\theta_1}{\Delta E} + F K_1 \frac{\Delta\theta_2}{\Delta E} + \left(1 - F \frac{K_2\theta_1}{F D_A} \frac{tanh\left(\delta\sqrt{\frac{j\omega}{D_A}}\right)}{\sqrt{\frac{j\omega}{D_A}}}\right) \frac{1}{Z_f F} = \\ \qquad F\left[\frac{\alpha_1 F}{RT} K_1 (1 - \theta_1 - \theta_2) + \frac{\alpha_2 F}{RT} K_2 [A]_0 \theta_1\right] \end{cases} \tag{32}$$

The faradaic impedance is then obtain as a solution of this system of 3 linear equations.

3.3. Parameters for the modelling

The fit of the parameters was performed using both Levenberg-Marquardt and step-by-step simplex regressions implemented in the measurement model tool developed by Orazem group.[36] Whatever the model considered, the number of parameters involved in the model is large. It is worth mentioning that the use of electrical equivalent circuit should also have resulted in a large number of parameters, with the added difficulty that it would then be very difficult to express any link between these parameters. However, a careful inspection of both systems of equations shows that some parameters are correlated. For the first step, it is not possible to determine independently K_1 and α_1, but one can only access to the product $K_1\alpha_1$. Similarly, for the second electrochemical step, it is not possible to determine K_2, α_1 and α_2, one can only get $K_2(\alpha_1 + \alpha_2)$, whereas for the chemical reaction, we can determine $K_d [B]_0$. Then for a global fitting of the experimental results, an interfacial capacitance (or a constant phase element, Q_{int}, α_{int}) has

to be added in parallel to the faradaic impedance, Z_f, as shown in Fig.1, together with the electrolyte resistance,R_{el}, in series. The electrolyte resistance was evaluated via the measurements model,[37] the other parameters or a combination of them were left free for the fitting procedure.

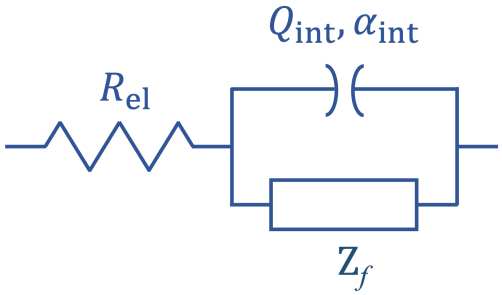

Figure 1: Electrical equivalent circuit used to analyse the EIS spectra. Z_f allows to introduce the analytical expression of the impedance that is derived from the electropolishing model presented in this work.

4. Results and discussion

Fig. 2 shows the anodic polarization curves of cast and ALM 316L performed at 2 mV s^{-1} in sulfuric acid solution (Fig. 2a) and in ChCl-EG (1:2) (Fig. 2b) at 70°C. Interestingly, the global shape of the curves in acidic solution and in DES are similar, only the current density and the length of the current plateau vary. Moreover, for both materials, curves remain unchanged in shape and allow to define 3 regions: the first one corresponds to the current increase and is ascribed to the active domain (dissolution of the alloys). The linear shape of the curves during the rise of the current when the potential increases is due to the uncompensated contribution of the ohmic drop (raw data without any compensation are presented in this figure). The second domain is a current plateau that spreads over 500 mV due to diffusion limited current. The last domain is characterized by a second increase in current, which is ascribed to the solvent and oxygen oxidation reactions. A first rough analysis of the experimental results therefore allows the conclusion that both alloys seems to follow a similar electrochemical behavior in the different electrolytes but with a shorter current plateau in acidic solutions than in DES. Moreover, the EP process that is usually performed at

a potential corresponding to the limiting current indicates that the global EP kinetics are similar for both materials. Additionally, the control of the dissolution reaction by diffusion was confirmed with the linear dependence of the limiting current density as a function of the electrode rotation rate as described by the Levich's law, as shown on Fig. 3. The limiting current is comparable for Cast and ALM materials and follows the same trend whatever the rotation rate and the media (DES and acidic solution). Moreover, in acidic media, varying the viscosity e.g. by changing temperature from 35°C to 70°C, shows a direct relationship between the diffusion coefficient and the kinematic viscosity, irrespective of the cation concentration at the interface, which suggest a minor role in the diffusion limiting step [19, 27]. This limitation is therefore ascribed to the diffusion of an acceptor species from the electrolyte toward the anode surface.

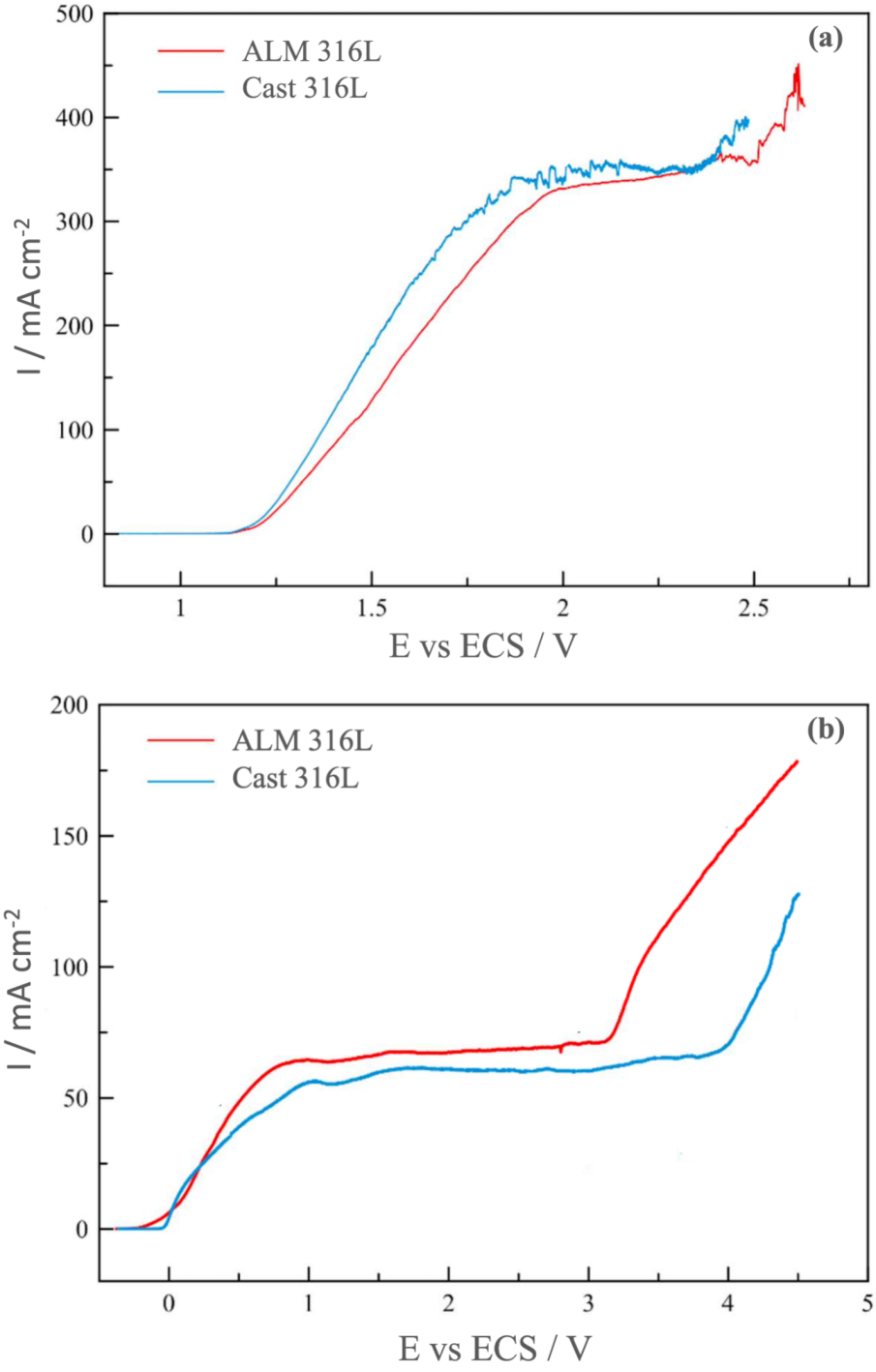

Figure 2: Polarization curves obtained for cast and ALM 316L at 2 mV s^{-1} and Ω= 500 rpm in acidic mixture (a) and in ChCl-EG (1:2) at 70°C (b)

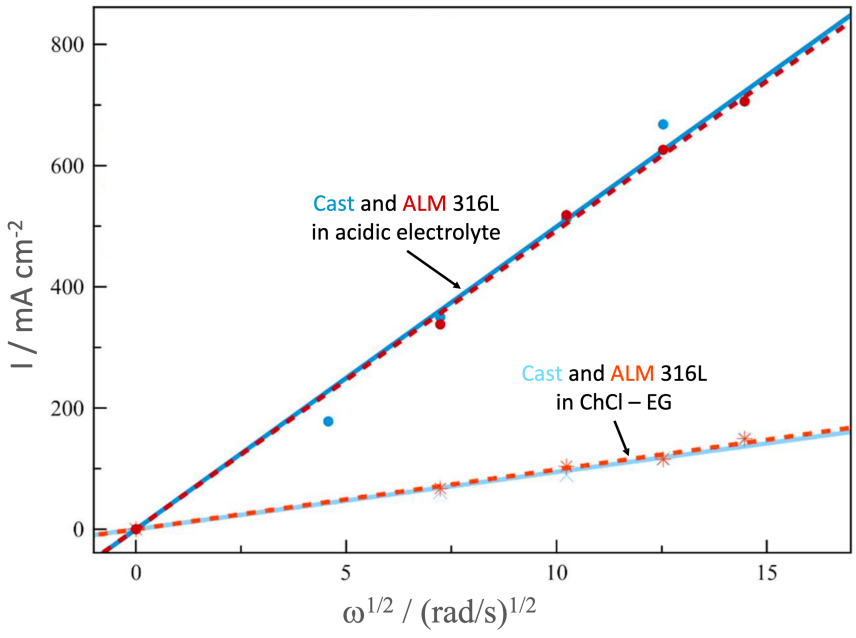

Figure 3: Levich's plot curves performed for cast and ALM 316L at 2 mV s^{-1} in ChCl-EG (1:2) and acidic mixture at 70°C

The manufacturing process used for the elaboration of materials is a parameter that strongly conditions the structural and functional properties of the items. SEM observations of the sample after the EP procedure are presented in Fig. 4, showing a smooth surface. However, a preliminary study has shown that for potentials corresponding to the zone of active dissolution, the substrate is etched according to certain preferential plane (anisotropic dissolution), whereas for a potential on the limiting-current plateau corresponding to a diffusion control mechanism, a smooth and bright surface was obtained for both samples and in both electrolytes without revealing the microstructure. The area roughness parameters (arithmetical mean height) determined by AFM measurements on 10 x 10 μm^2 were between 1 and 2 nm for all the samples, with a maximum peak-to-valley height of 80 nm [12].

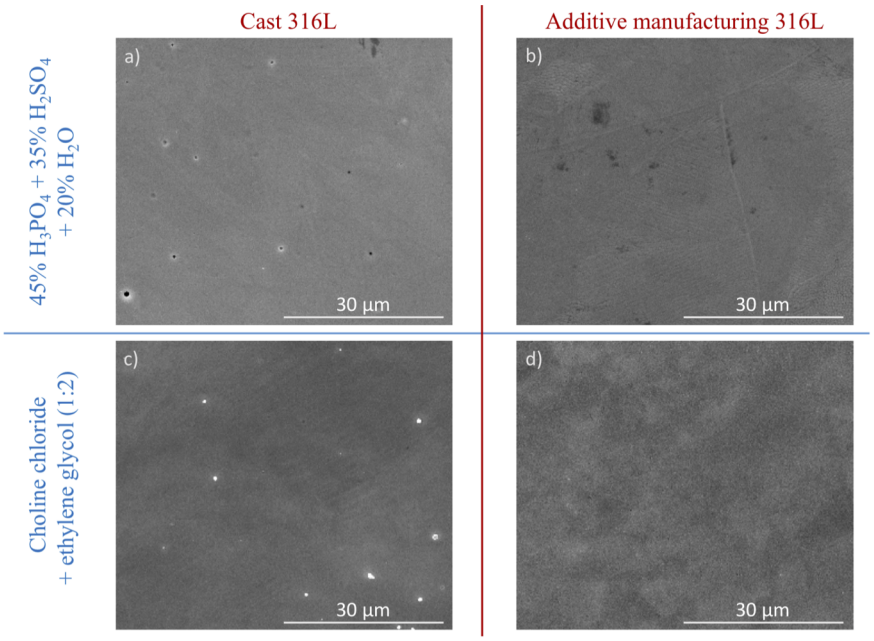

279

Figure 4: SEM observations of the samples after EP procedure at 70°C - 500 rpm. a) and
280 b) at 2.4 V/SCE, c) and d) at 3 V/SCE

281 EIS diagrams obtained for both materials in DES at 70°C are presented
282 in Fig. 5 for experiments performed at 0.4 V/SCE and 2.1 V/SCE. The EIS
283 response depends on the applied potential but is independent of the ma-
284 terials. Three time constants can be observed on these diagrams: a high
285 frequency capacitive semi-circle corresponding to the charge transfer resis-
286 tance in parallel with the capacitance of the interface, an inductive behavior
287 that may be ascribed either to the relaxation of adsorbed species or to the
288 relaxation of the thickness of corrosion-product layer with the potential, and
289 a low frequency time constant that can originate from diffusion process and
290 the relaxation of chemical steps. It should also be mentioned that the high
291 frequency domain shows a 45° slope that spreads over a larger frequency do-
292 main in DES (Fig. 5a) than in acidic solution (an example of EIS diagrams
293 in adic media is presented in Fig. 7), and that also depends on the applied
294 potential, thus indicating the formation of a porous layer which is thicker at

higher potential in DES (Fig. 5b).

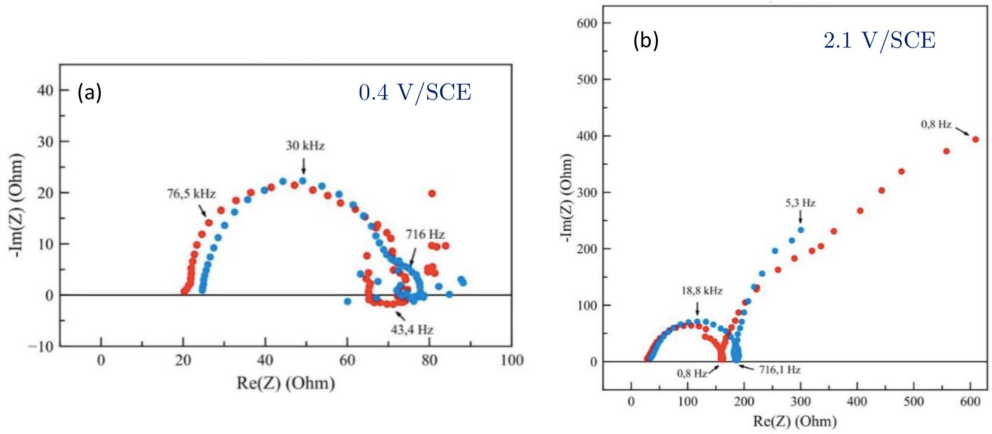

Figure 5: Experimental EIS diagrams for Cast (blue circles) and ALM (red circles) 316L SS electropolished in ChCl-EG at 70°C at 0.4 V/SCE (a) and 2.1 V/SCE (b)

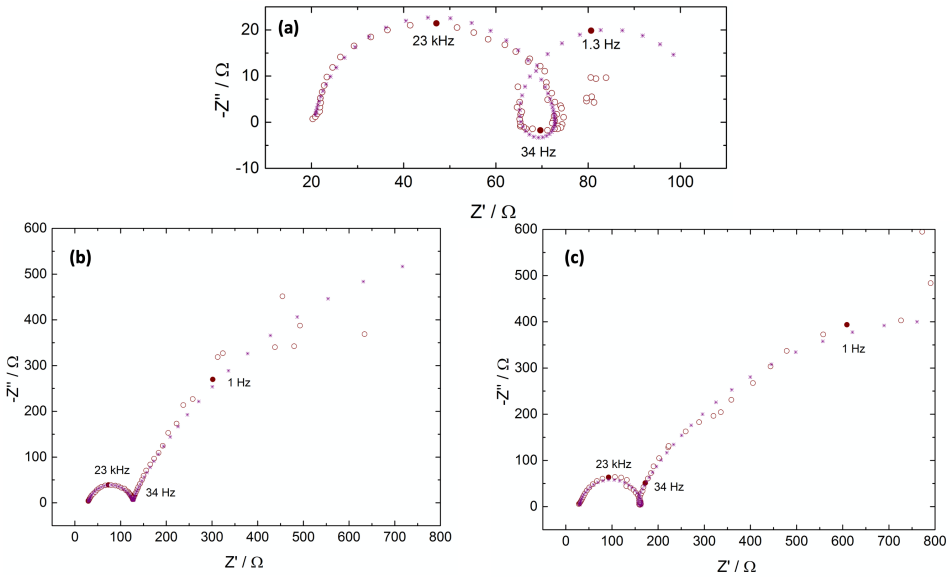

Figure 6: Experimental and calculated EIS diagrams for ALM 316L SS electropolished in ChCl-EG at 70°C at (a) 0.4 V/SCE; (b) 1.2 V/SCE; and (c) 2.1 V/SCE. Circles: experimental data; crosses: fit

Fig. 6 shows experimental and calculated EIS diagrams for ALM 316L SS electropolished in ChCl-EG at 70°C as a function of the potential. The low

frequency range was limited to the Hz domain since the response was noisy due to the evolution of the interface as a function of time. The two models in which either water or an acceptor specie is assumed to be the limiting specie were considered, but the comparison between fitting and experimental results lead to the validation of the acceptor specie model, as shown with the fit results presented in Fig. 6. The fitted parameters presented in Tables 3 and 4 show that the interfacial capacitance, C_{eff}, is systematically smaller than the value expected for a double layer capacitance (generally in the range of 10 µF cm^2), which indicates the formation of a thin layer of corrosion products (about 100-200 nanometers at 0.4 V/SCE) whose thickness increases with the polarization potential of the electrode. It was also observed that the electrolyte resistance, which is dependent on the system geometry and the conductivity of the solution, increases slightly with potential. This variation can be explained in two ways: on the one hand by a variation in electrolyte conductivity due to the dissolution of material (the dissolution of the metal is accompanied by the consumption of ions of the solution, thus forming complexes), and on the other hand by a resistive contribution due to corrosion products on the electrode surface which is added to the resistance measured at high frequency. Theses variations for the electrolyte resistance and the interfacial capacitance are in agreement with the porous behavior of the electrode previously described in the high frequency domain. The desorption rate constant measured by the product $K_d C_B$ (Tables 3 and 4) tends towards a constant value when the potential increases, showing that this chemical step is a kinetic limitation in the EP process. The variations of the charge transfer resistance is also in agreement with the dissolution curve. It is higher on the plateau (smaller current) and larger on the active dissolution domain (i.e. a 0.4 V/SCE).

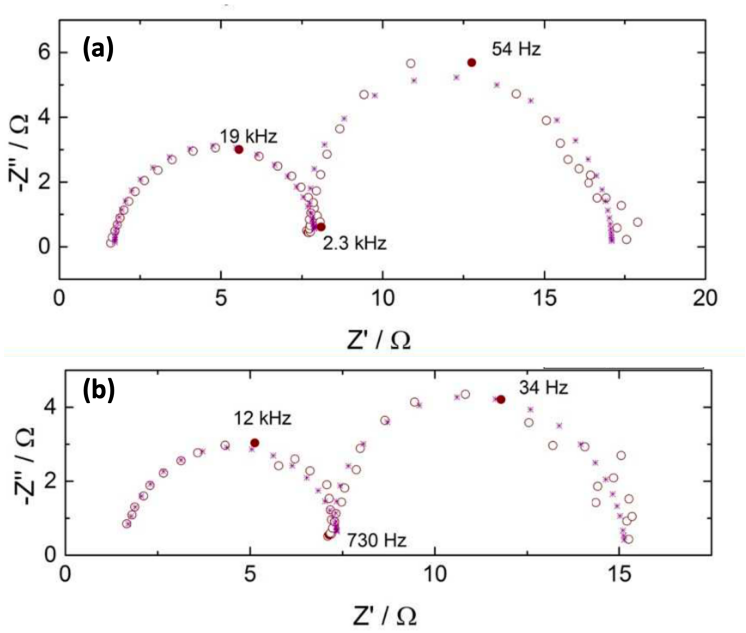

Figure 7: Experimental and calculated EIS diagrams for cast (a) and ALM 316L SS (b) electropolished in acidic solution at 2.1 V/SCE. Circles: experimental data; crosses: fit

Table 3: Kinetic parameters obtained from the fitting procedure for the cast 316L in DES

Potential (V/SCE)	0.4	1.2	2.1
Interfacial capacitance C_{eff} (µF cm^2)	10.2 ± 0.5	0.15 ± 0.01	0.10 ± 0.01
Step 1 $K_1\alpha_1$	(3 ± 0.2) 10^{-1}	(4.3 ± 0.3)	(5.9 ± 0.3)
Step 2 $K_2(\alpha_1 + \alpha_2)$	(8.7 ± 0.4) 10^{-5}	(4.3 ± 0.2) 10^{-3}	(4.8 ± 0.3) 10^{-3}
Desorption step K_dC_B	(3.4 ± 0.2) 10^{-4}	(7 ± 0.5) 10^{-4}	(6.9 ± 0.5) 10^{-4}

Interestingly, the same conclusions can be drawn for the analyses of the EP treatments carried out in concentrated acid medium for both materials as shown for the EIS diagrams presented in Fig. 7. The shape of the impedance diagrams is very similar to the one obtained in DES at the same potential (E = 2.1 V/SCE), but the two low-frequency time constants, namely the inductive time constant the kHz range and the capacitive time constant around the tenth of Hz, are shifted towards higher frequency domain when the polishing was performed in aqueous solution. These experimental data were analyzed

Table 4: Kinetic parameters obtained from the fitting procedure for the ALM 316L in DES

Potential (V/SCE)	0.4	1.2	2.1
Interfacial capacitance C_{eff} (µF cm^2)	0.20 ± 0.01	0.12 ± 0.01	0.10 ± 0.01
Step 1 $K_1\alpha_1$	(4.5 ± 0.2) 10^{-2}	(3.0 ± 0.2)	(6.1 ± 0.7)
Step 2 $K_2(\alpha_1 + \alpha_2)$	(5.4 ± 0.3) 10^{-4}	(9.9 ± 0.3) 10^{-4}	(9.3 ± 0.4) 10^{-5}
Desorption step K_dC_B	(3.2 ± 0.1) 10^{-5}	(3.2 ± 0.2) 10^{-3}	(3.2 ± 0.2) 10^{-3}

using the same model than the one used for the analysis of results obtained in DES and the fitted parameters are presented in Tables 5. The value of the interfacial capacitance (larger than 1 µF cm^2) is significantly higher than in the case of an EP in the DES, which is consistent with either a double layer capacitance for a metal/electrolyte interface in highly concentrated solution, or with a combination in series of a capacitance ascribed to a very thin corrosion product layer in series with the double layer capacitance. It is therefore deduced that the proposed mechanism makes it possible to account for electropolishing in the most commonly used media (acid solutions) but also in new solvents which are increasingly used because of their eco-friendly nature.

Table 5: Kinetic parameters obtained from the fitting procedure for the cast and ALM 316L in acidic electrolyte at 2.1 V/SCE

	Cast 316L	ALM 316L
Interfacial capacitance C_{eff} (µF cm^2)	1.10 ± 0.04	1.90 ± 0.06
Step 1 $K_1\alpha_1$	(7.9 ± 0.4) 10^2	(4.2 ± 0.3) 10^2
Step 2 $K_2(\alpha_1 + \alpha_2)$	(7.7 ± 0.5) 10^{-4}	(1.7 ± 0.2) 10^{-4}
Desorption step K_dC_B	(1.2 ± 0.1) 10^{-6}	(2.7 ± 0.1) 10^{-6}

5. Conclusions

This study has showed with the analysis of the experimental electrochemical impedance diagrams that the model involving an acceptor specie enables to describe all the results obtained for the two materials, namely the cast 316L and the ALM 316L. The proposed mechanism makes it possible to describe, from a kinetic point a view, the electropolishing process for concentrated acidic media and DES. However, as the number of variables is large and since they depend on each other, only combinations of these parameters can be obtained from the analysis of impedance spectra and the fitting procedure. It should be noted, however, that the value of the interfacial capacitance measured in the case of electropolishing in DES can be linked to the formation of a corrosion product thin film, which also results in a slight increase of the electrolyte resistance.

Acknowledgements

Chloé Rotty gratefully acknowledges financial support from the program "MoMeQa Innovation Stratégique Industrielle ISI" and BPI France. The authors are grateful to Mr. N. Rouge, PCU UTINAM plateform for his help on SEM images.

References

[1] W. E. Frazier, Metal additive manufacturing: A review, Journal of Materials Engineering and Performance 23 (6) (2014) 1917–1928. doi:10.1007/s11665-014-0958-z.

[2] S. M. Thompson, L. Bian, N. Shamsaei, A. Yadollahi, An overview of direct laser deposition for additive manufacturing; part i: Transport phenomena, modeling and diagnostics, Additive Manufacturing 8 (2015) 36–62. doi:10.1016/j.addma.2015.07.001.

[3] N. Shamsaei, A. Yadollahi, L. Bian, S. M. Thompson, An overview of direct laser deposition for additive manufacturing; part ii: Mechanical behavior, process parameter optimization and control, Additive Manufacturing 8 (2015) 12–35. doi:10.1016/j.addma.2015.07.002.

[4] A. K. Au, W. Huynh, L. F. Horowitz, A. Folch, 3d-printed microfluidics, Angewandte Chemie - International Edition 55 (12) (2016) 3862–3881. doi:10.1002/anie.201504382.

[5] E. O. Olakanmi, R. F. Cochrane, K. W. Dalgarno, A review on selective laser sintering/melting (sls/slm) of aluminium alloy powders: Processing, microstructure, and properties, Progress in Materials Science 74 (2015) 401–477. doi:10.1016/j.pmatsci.2015.03.002.

[6] J. H. Tan, W. L. E. Wong, K. W. Dalgarno, An overview of powder granulometry on feedstock and part performance in the selective laser melting process, Additive Manufacturing 18 (2017) 228–255. doi:10.1016/j.addma.2017.10.011.

[7] J. L. Bartlett, X. Li, An overview of residual stresses in metal powder bed fusion, Additive Manufacturing 27 (2019) 131–149. doi:10.1016/j.addma.2019.02.020.

[8] D. Landolt, Fundamental aspects of electropolishing, Electrochimica Acta 32 (1) (1987) 1 – 11. doi:https://doi.org/10.1016/0013-4686(87)87001-9.

[9] W. Han, F. Fang, Fundamental aspects and recent developments in electropolishing, International Journal of Machine Tools and Manufacture 139 (2019) 1 – 23. doi:10.1016/j.ijmachtools.2019.01.001.

[10] A. P. Abbott, G. Capper, K. J. McKenzie, A. Glidle, K. S. Ryder, Electropolishing of stainless steels in a choline chloride based ionic liquid: an electrochemical study with surface characterisation using sem and atomic force microscopy, Phys. Chem. Chem. Phys. 8 (2006) 4214–4221. doi:10.1039/B607763N.

[11] C. Rotty, M.-L. Doche, A. Mandroyan, J.-Y. Hihn, Electropolishing behavior of additive layer manufacturing 316l stainless steel in deep eutectic solvents, ECS Transactions 77 (11) (2017) 1199–1207. doi:10.1149/07711.1199ecst.

[12] C. Rotty, A. Mandroyan, M.-L. Doche, S. Monney, J.-Y. Hihn, N. Rouge, Electrochemical superfinishing of cast and alm 316l stainless steels in deep eutectic solvents: Surface microroughness evolution and corrosion resistance, Journal of the Electrochemical Society 166 (13) (2019) C468–C478. doi:10.1149/2.1211913jes.

[13] W. Han, F. Fang, Two-step electropolishing of 316l stainless steel in a sulfuric acid-free electrolyte, Journal of Materials Processing Technology 279 (2020) 116558. doi:10.1016/j.jmatprotec.2019.116558.

[14] A. Awad, N. A. Ghany, T. Dahy, Removal of tarnishing and roughness of copper surface by electropolishing treatment, Applied Surface Science 256 (13) (2010) 4370 – 4375. doi:10.1016/j.apsusc.2010.02.033.

[15] C. A. Huang, J. H. Chang, W. J. Zhao, S. Y. Huang, Examination of the electropolishing behaviour of 73 brass in a 70rotating disc electrode, Materials Chemistry and Physics 146 (3) (2014) 230 – 239. doi:10.1016/j.matchemphys.2014.02.052.

[16] C. Rotty, A. Mandroyan, M.-L. Doche, J. Hihn, Electropolishing of cuzn brasses and 316l stainless steels: Influence of alloy composition or preparation process (alm vs. standard method), Surface and Coatings Technology 307 (2016) 125 – 135. doi:10.1016/j.surfcoat.2016.08.076.

[17] R. Sautebin, H. Froidevaux, D. Landolt, Theoretical and experimental modeling of surface leveling in ECM under primary current distribution conditions, Journal of The Electrochemical Society 127 (5) (1980) 1096. doi:10.1149/1.2129823.

[18] R. Sautebin, D. Landolt, Anodic leveling under secondary and tertiary current distribution conditions, Journal of The Electrochemical Society 129 (5) (1982) 946. doi:10.1149/1.2124071.

[19] C. Clerc, D. Landolt, On the theory of anodic levelling: Fem simulation of the influence of profile shape and cell geometry, Electrochimica Acta 29 (6) (1984) 787 – 795. doi:10.1016/0013-4686(84)80015-8.

[20] P. Jacquet, A new method of achieving perfectly polished metallic surfaces, Comptes Rendus Hebdomadaires des Seances de l'Academie des Sciences 201 (1935) 1473–1475.

[21] P. Jacquet, Regarding the electrolytic polishing of aluminum, Comptes Rendus Hebdomadaires des Seances de l'Academie des Sciences 205 (1937) 1232–1235.

[22] W. Elmore, Electrolytic polishing, Journal of Applied Physics 10 (10) (1939) 724–727. doi:10.1063/1.1707257.

[23] W. Elmore, Electrolytic polishing II, Journal of Applied Physics 11 (12) (1940) 797–799. doi:10.1063/1.1712738.

[24] C. Wagner, Contribution to the theory of electropolishing, Journal of The Electrochemical Society 101 (5) (1954) 225. doi:10.1149/1.2781235.

[25] J. Edwards, The mechanism of electropolishing of copper in phosphoric acid solutions, Journal of The Electrochemical Society 100 (8) (1953) 223C. doi:10.1149/1.2781129.

[26] J. Edwards, The mechanism of electropolishing of copper in phosphoric acid solutions, Journal of The Electrochemical Society 100 (7) (1953) 189C. doi:10.1149/1.2781122.

[27] M. Matlosz, Modeling of impedance mechanisms in electropolishing, Electrochimica Acta 40 (4) (1995) 393–401. doi:10.1016/0013-4686(94)00287-B.

[28] M. Bojinov, I. Betova, G. Fabricius, T. Laitinen, R. Raicheff, Passivation mechanism of iron in concentrated phosphoric acid, Journal of Electroanalytical Chemistry 475 (1) (1999) 58–65. doi:10.1016/S0022-0728(99)00343-5.

[29] O. E. Barcia, O. R. Mattos, B. Tribollet, , Journal of The Electrochemical Society 139 (2) (1992) 446. doi:10.1149/1.2069238.
URL

[30] I. Epelboin, M. Keddam, J. C. Lestrade, Faradaic impedances and intermediates in electrochemical reactions, Faraday Discuss. Chem. Soc. 56 (1973) 264–275. doi:10.1039/DC9735600264.

[31] I. Epelboin, M. Keddam, O. Mattos, H. Takenouti, The dissolution and passivation of fe and fecr alloys in acidified sulphate medium: Influences of ph and cr content, Corrosion Science 19 (7) (1979) 1105 – 1112. doi:10.1016/S0010-938X(79)80099-2.

[32] C. Cachet, F. Ganne, G. Maurin, J. Petitjean, V. Vivier, R. Wiart, EIS investigation of zinc dissolution in aerated sulfate medium. Part I: bulk zinc, Electrochimica Acta 47 (3) (2001) 509–518. doi:10.1016/S0013-4686(01)00740-X.

[33] M. P. Gomes, I. Costa, N. Pébère, J. L. Rossi, B. Tribollet, V. Vivier, On the corrosion mechanism of mg investigated by electrochemical impedance spectroscopy, Electrochimica Acta 306 (2019) 61 – 70. doi:10.1016/j.electacta.2019.03.080.

[34] M. E. Orazem, B. Tribollet, Electrochemical Impedance Spectroscopy, 2nd Edition, The ECS Series of Texts and Monographs, Wiley, Hoboken, NJ, 2017.

[35] I. D. Raistrick, J. R. Macdonald, D. R. Franceschetti, Theory *in*

Impedance Spectroscopy, John Wiley & Sons, Ltd, 2018, Ch. 2, pp. 21–105. doi:10.1002/9781119381860.ch2.

[36] W. Watson, M. E. Orazem, EIS: Measurement model program (Sep 2020).
URL ecsarxiv.org/kze9x

[37] H. Liao, W. Watson, A. Dizon, B. Tribollet, V. Vivier, M. E. Orazem, Physical properties obtained from measurement model analysis of impedance measurements, Electrochimica Acta 354 (2020) 136747. doi:10.1016/j.electacta.2020.136747.

List of Symbols

- C_{dl}: double layer capacitance (in µF cm^2)
- C_{eff}: interfacial capacitance (in µF cm^2)
- C_s: concentration of the species s (in mol L^{-1})
- D_s: diffusion coefficient of the species s (in cm^2 s^{-1})
- E: Electrode potential (in V)
- f: frequency (in Hz)
- F: Faraday's constant (96485 C mol^{-1})
- i: current density (in A cm^{-2})
- k_i: kinetic constant of reaction i linked to K_i via Eq. (3) (in cm^{-2} s^{-1}
- K_i: kinetic constant of reaction i (in cm^{-2} s^{-1})
- p: variable in the Laplace domain
- Q_{int}: constant-phase-element parameter (in F/s$^{(1-\alpha_{int})}$ cm^2)
- r: radius of the electrode (in cm)
- R: gas constant (8.314 J K^{-1} mol^{-1})
- R_{el}: electrolyte resistance (in Ω cm^2)
- T: temperature (in K)
- v_i: rate of the reaction i
- Y: admittance (in S cm^{-2})
- Z: impedance (in Ω cm^2)
- Z_f: faradaic impedance (in Ω cm^2)
- α_i: charge transfer coefficient of reaction i
- α_{int}: constant-phase-element parameter

- β: surface concentration for complete coverage (in mol cm^{-2})
- η: dynamic viscosity (in Pa s)
- ν: kinematic viscosity (in cm^2 s^{-1})
- ρ: density (in g cm^{-3})
- σ: conductivity (in S cm^{-1})
- θ_1: surface coverage of MA^+_{ads}
- θ_2: surface coverage of MA^{2+}_{ads}
- ω: angular frequency (in rad s^{-1})
- Ω: rotation rate of the RDE (in rad s^{-1})

List of Figures